

# Two Photon Decays of $\eta_c$ from Lattice QCD

Ting Chen,<sup>1</sup> Ying Chen,<sup>2</sup> Ming Gong,<sup>2</sup> Yu-Hong Lei,<sup>1</sup> Ning Li,<sup>3</sup> Chuan Liu,<sup>4, 5, \*</sup>  
Yu-Bin Liu,<sup>6</sup> Zhaofeng Liu,<sup>2</sup> Jian-Ping Ma,<sup>7</sup> Zhan-Lin Wang,<sup>1</sup> and Jian-Bo Zhang<sup>8</sup>  
(CLQCD Collaboration)

<sup>1</sup>*School of Physics, Peking University, Beijing 100871, China*

<sup>2</sup>*Institute of High Energy Physics, Chinese Academy of Sciences, Beijing 100049, China*

<sup>3</sup>*School of Science, Xi'an Technological University, Xi'an 710032, China*

<sup>4</sup>*School of Physics and Center for High Energy Physics, Peking University, Beijing 100871, China*

<sup>5</sup>*Collaborative Innovation Center of Quantum Matter, Beijing 100871, China*

<sup>6</sup>*School of Physics, Nankai University, Tianjin 300071, China*

<sup>7</sup>*Institute of Theoretical Physics, Chinese Academy of Sciences, Beijing 100190, China*

<sup>8</sup>*Department of Physics, Zhejiang University, Hangzhou 311027, China*

We present an exploratory lattice study for the two-photon decay of  $\eta_c$  using  $N_f = 2$  twisted mass lattice QCD gauge configurations generated by the European Twisted Mass Collaboration. Two different lattice spacings of  $a = 0.067\text{fm}$  and  $a = 0.085\text{fm}$  are used in the study, both of which are of physical size of  $2\text{fm}$ . The decay widths are found to be  $1.113(63)\text{KeV}$  for the finer lattice and  $0.961(59)\text{KeV}$  for the coarser lattice respectively where the errors are purely statistical. A naive extrapolation towards the continuum limit yields  $\Gamma \simeq 1.36(19)\text{KeV}$  which is smaller than, but marginally compatible with previous quenched result and the current experimental result.

## I. INTRODUCTION

Charmonium systems play a major role in the understanding of the foundation of quantum chromodynamics (QCD). Due to its intermediate energy scale and the special features of QCD, both perturbative and non-perturbative physics show up within charmonium physics, making it an ideal testing ground for our understanding of QCD from both sides.

Two-photon decay width of  $\eta_c$  has been attracting considerable attention over the years from both theory and experiment sides. For example, it is related to the process  $gg \rightarrow \eta_c$  relevant for charmonia production at LHC and the small- $x$  gluon distribution function from the inclusive production of  $\eta_c$  which describes the non-leptonic B mesons decays [1]. Furthermore, two-photon branching fraction for charmonium provides a probe for the strong coupling constant at the charmonium scale via the two-photon decay widths, which can be utilized as a sensitive test for the corrections for the non-relativistic approximation in the quark models or the effective field theories such as non-relativistic QCD (NRQCD).

On the experimental side, considerable progress has been made in recent years in the physics of charmonia via the investigations from Belle, BaBar, CLEO-c and BES [2–5]. Two methods can be utilized to measure the two-photon branching fraction for charmonium. One is reconstructing the charmonium in light hadrons with two-photon fusion at  $e^+e^-$  machines. The other one is to make  $p\bar{p}$  pairs annihilated to charmonium with decay and then to detect the real  $\gamma\gamma$  pairs. Improvements of measuring two-photon branching fraction for charmonia

will soon reached via more accurate measurements from experimental progress.

On the theoretical side, charmonium electromagnetic transitions have been investigated using various theoretical methods [6–14]. In principle, these processes involve both electromagnetic and strong interactions, the former being perturbative in nature while the latter being non-perturbative. Therefore, the study for charmonium transitions requires non-perturbative theoretical methods such as lattice QCD. Hadronic matrix element computations are standard in lattice QCD, however, processes involving initial or final photons are a bit more subtle. Since photons are not QCD eigenstates, one has to rely on perturbative methods to “replace” the photon states by the corresponding electromagnetic currents that they couple to. The details of this idea was illustrated in Ref. [15, 16]. Using this technique, the first *ab initio* quenched lattice calculation of two photon decay of charmonia was reported in Ref. [17]. They found reasonable agreement with the experimental world-average values for  $\eta_c$  and  $\chi_{c0}$  decay rates. However, an unquenched lattice study is still lacking. In this paper, we would like to fill this gap by computing the two photon decay rates of  $\eta_c$  meson in lattice QCD with  $N_f = 2$  flavors of light quarks in the sea. The gauge configurations are generated by the European Twisted Mass Collaboration (ETMC) [18–29], where the twisted mass fermion parameters are set at the maximal twist. This ensures the automatic  $\mathcal{O}(a)$  improvement for on-shell observables where  $a$  is the lattice spacing [30].

This paper is organized as follows. In Section II, we briefly review the calculation strategies for the matrix element for two-photon decay of  $\eta_c$ . The following section III are divided into three parts containing details of the simulation: In section III A, we introduce the twist mass fermion formulation and give the parameters of the lattices used in our simulation. In section III C, the con-

\* Corresponding author. Email: liuchuan@pku.edu.cn

tinuum and lattice dispersion relations for  $\eta_c$  are checked. In section III D, numerical results of the form factor are presented which are then converted to the decay width of  $\eta_c$  meson. In Section IV, we concluded our discussions.

## II. STRATEGIES FOR THE COMPUTATION

In this section, we briefly recapitulate the methods for the calculation of two-photon decay rate of  $\eta_c$  presented in Ref. [17]. The amplitude for two-photon decay of  $\eta_c$  can be expressed in terms of a photon two-point function in Minkowski space by means of the Lehmann-Symanzik-Zimmermann (LSZ) reduction formula up to photon renormalization factors,

$$\langle \gamma(q_1, \lambda_1) \gamma(q_2, \lambda_2) | \eta_c(p) \rangle = - \lim_{\substack{q'_1 \rightarrow q_1 \\ q'_2 \rightarrow q_2}} \epsilon_\mu^*(q_1, \lambda_1) \epsilon_\nu^*(q_2, \lambda_2) q_1'^2 q_2'^2 \int d^4x d^4y e^{iq'_1 \cdot y + iq'_2 \cdot x} \langle \Omega | T \{ A^\mu(y) A^\nu(x) \} | \eta_c(p_f) \rangle. \quad (1)$$

Here  $|\Omega\rangle$  designates the QCD vacuum state,  $|\eta_c(p)\rangle$  is the state with an  $\eta_c$  meson of four-momentum  $p$  and  $|\gamma(q_i, \lambda_i)\rangle$  for  $i = 1, 2$  denote a single photon state with corresponding polarization vector  $\epsilon(q_i, \lambda_i)$ . Then one uti-

lizes the perturbative nature of the photon-quark coupling to approximately integrate out the photon fields and rewrites the corresponding path-integral as,

$$\int \mathcal{D}A \mathcal{D}\bar{\psi} \mathcal{D}\psi e^{iS_{QED}[A, \bar{\psi}, \psi]} A^\mu(y) A^\nu(x) = \int \mathcal{D}A \mathcal{D}\bar{\psi} \mathcal{D}\psi e^{iS_0[A, \bar{\psi}, \psi]} \left( \dots + \frac{e^2}{2} \int d^4z d^4w \right. \\ \left. \times [\bar{\psi}(z) \gamma^\rho \psi(z) A_\rho(z)] [\bar{\psi}(w) \gamma^\sigma \psi(w) A_\sigma(w)] + \dots \right) A^\mu(y) A^\nu(x). \quad (2)$$

The integration over the photon fields can be carried out by Wick contracting the fields into propagators. Neglect-

ing the disconnected diagrams, one arrives at the following equation,

$$\langle \gamma(q_1, \lambda_1) \gamma(q_2, \lambda_2) | \eta_c(p) \rangle = (-e^2) \lim_{\substack{q'_1 \rightarrow q_1 \\ q'_2 \rightarrow q_2}} \epsilon_\mu^*(q_1, \lambda_1) \epsilon_\nu^*(q_2, \lambda_2) q_1'^2 q_2'^2 \int d^4x d^4y d^4w d^4z e^{iq'_1 \cdot y + iq'_2 \cdot x} D^{\mu\rho}(y, z) D^{\nu\sigma}(x, w) \\ \times \langle \Omega | T \{ j_\rho(z) j_\sigma(w) \} | \eta_c(p_f) \rangle. \quad (3)$$

In this equation,

$$D^{\mu\nu}(y, z) = -ig^{\mu\nu} \int \frac{d^4k}{(2\pi)^4} \frac{e^{-ik \cdot (y-z)}}{k^2 + i\epsilon}, \quad (4)$$

is the free photon propagator, which in momentum space will cancel out the inverse propagators outside the integral in Eq. (1) and Eq. (3) when the limit is taken. The current operators such as  $j_\rho(x) = Z_V(g_0^2) \bar{c}(x) \gamma_\rho c(x)$  is the vector current of the charm quark with  $c(x)/\bar{c}(x)$  being the bare charm/anti-charm quark field on the lattice. Contributions due to other quark flavors, e.g. up, down or strange, only come in via disconnected diagrams which are neglected in this exploratory study. Annihilation diagrams of the charm quark itself are also neglected due to OZI-suppression. In fact, in our twisted mass lattice

setup, we introduce two different charm quark fields with degenerate masses, so that this type of diagram is absent, see subsection III A.

We remark that a renormalization constant  $Z_V(g_0^2)$  is needed since we are using the non-conserving local current operator on the lattice. These factors have been computed by the ETMC collaboration [31]. To be specific, for the two set of lattices used in this study, the values of the renormalization factor  $Z_V(g_0^2)$  are 0.6103(3) and 0.6451(3) for the lattice size  $24^3 \times 48$  at  $\beta = 3.9$  and  $32^3 \times 64$  at  $\beta = 4.05$ , respectively.

The resulting expression (3) can then be analytically continued from Minkowski to Euclidean space. This continuation works as long as none of the  $q_i^2$  is too time-like. To be precise, the continuation is fine as long as the virtu-

alities of the two photons  $Q_i^2 \equiv (-q_i^2) > -M_V^2$  where  $M_V$  is the mass of the lightest vector meson in QCD [15, 17]. For quenched lattice QCD, the lightest vector meson is  $J/\psi$ . However, for our unquenched study, it is safe to take  $M_V = m_\rho$ , i.e. the mass of the  $\rho$  meson. Using

$$\langle \eta_c(p_f) | \gamma(q_1, \lambda_1) \gamma(q_2, \lambda_2) \rangle = \lim_{t_f - t \rightarrow \infty} e^2 \frac{\epsilon_\mu(q_1, \lambda_1) \epsilon_\nu(q_2, \lambda_2)}{\frac{Z_{\eta_c}(\mathbf{p}_f)}{2E_{\eta_c}(\mathbf{p}_f)} e^{-E_{\eta_c}(\mathbf{p}_f)(t_f - t)}} \int dt_i e^{-\omega_1(t_i - t)} \left\langle \Omega \left| T \left\{ \int d^3\mathbf{x} e^{-i\mathbf{p}_f \cdot \mathbf{x}} \mathcal{O}_{\eta_c}(\mathbf{x}, t_f) \int d^3\mathbf{y} e^{i\mathbf{q}_2 \cdot \mathbf{y}} j^\nu(\mathbf{y}, t) j^\mu(\mathbf{0}, t_i) \right\} \right| \Omega \right\rangle, \quad (5)$$

where  $\mathcal{O}_{\eta_c}(x)$  is an interpolating operator that will create an  $\eta_c$  meson from the vacuum and  $\omega_1$  is the energy of the first photon. The kinematics in this equation is such that four-momentum conservation  $p_f = q_1 + q_2$  is valid. This equation serves as the starting point for our subsequent lattice computation. Basically, the current that couples to the first photon is placed at the source time-slice  $t_i$ , the second current is at  $t$  while the final  $\eta_c$  meson is at the sink time-slice  $t_f$  and we are led to the computation of a three-point function of the form

$$C(\mathbf{p}_f; t) \equiv \sum_{\mathbf{x}} e^{-i\mathbf{p}_f \cdot \mathbf{x}} \langle \Omega | \mathcal{O}_{\eta_c}(\mathbf{x}, t) \mathcal{O}_{\eta_c}^\dagger(\mathbf{0}, 0) | \Omega \rangle \xrightarrow{t \gg 1} \frac{|Z_{\eta_c}(\mathbf{p}_f)|^2}{E_{\eta_c}(\mathbf{p}_f)} e^{-E_{\eta_c}(\mathbf{p}_f) \cdot \frac{T}{2}} \cosh \left[ E_{\eta_c}(\mathbf{p}_f) \cdot \left( \frac{T}{2} - t \right) \right], \quad (6)$$

where  $Z_{\eta_c}(\mathbf{p}_f) = \langle \Omega | \mathcal{O}_{\eta_c} | \eta_c(\mathbf{p}_f) \rangle$  is the corresponding overlap matrix element.

suitable interpolating operator (denoted by  $\mathcal{O}_{\eta_c}(x)$ ) to create an  $\eta_c$  meson from the vacuum and reversing the operator time-ordering for later convenience, we finally obtain,

$\langle \Omega | \mathcal{O}_{\eta_c}(\mathbf{x}, t_f) j^\nu(\mathbf{y}, t) j^\mu(\mathbf{0}, t_i) | \Omega \rangle$ . Of course, one has to compute the above three-point functions for each  $t_i$  and perform an integration (summation) over  $t_i$ .

Apart from the above mentioned three-point functions, we also need information from  $\eta_c$  two-point function. For example, in the above equation,  $Z_{\eta_c}(p_f)$  is the spectral weight factor while  $E_{\eta_c}(p_f)$  is the energy for  $\eta_c$  with four-momentum  $p_f = (E_{\eta_c}, \mathbf{p}_f)$ . These can be inferred from the corresponding two-point functions for  $\eta_c$ . For this purpose, two-point correlation functions for the interpolating operators  $\mathcal{O}_{\eta_c}$  are computed in the simulation:

The three-point functions, denoted by  $G_{\mu\nu}(t_i, t)$ , that need to be computed in our simulation are of the form,

$$G_{\mu\nu}(t_i, t) = \left\langle \Omega \left| T \left\{ \int d^3\mathbf{x} e^{-i\mathbf{p}_f \cdot \mathbf{x}} \mathcal{O}_{\eta_c}(\mathbf{x}, t_f) \int d^3\mathbf{y} e^{i\mathbf{q}_2 \cdot \mathbf{y}} j^\nu(\mathbf{y}, t) j^\mu(\mathbf{0}, t_i) \right\} \right| \Omega \right\rangle. \quad (7)$$

Keeping the sink of  $\eta_c$  fixed at  $t_f = T/2$ , we compute  $G_{\mu\nu}(t_i, t)$  across the temporal direction for all  $t_i$  and  $t$  on our lattices. For a fixed  $t_i$ , one has to use sequential source technique to obtain the  $t$  dependence of the three-point function. Then, the same calculation is repeated with a varying  $t_i$ . Then, according to Eq. (5), the desired matrix element is obtained by using the results of  $G_{\mu\nu}(t_i, t)$  for different combinations of  $t_i$  and  $t$  and integrate over  $t_i$  with an exponential weight  $e^{-\omega_1 t_i}$ . In practice, the integral is replaced by a summation over  $t_i$ . To explore the validity of this replacement, we have checked the behavior of the integrand some of which are illustrated in Fig. 2.

### III. SIMULATION DETAILS

#### A. Simulation setup

In this study, we use twisted mass fermions at the maximal twist. The most important advantage of this setup is the so-called automatic  $\mathcal{O}(a)$  improvement for the physical quantities. To be specific, we use  $N_f = 2$  (degenerate  $u$  and  $d$  quark) twisted mass gauge field configurations generated by the European Twisted Mass Collaboration (ETMC). The other quark flavors, namely strange and charm quarks, are quenched. These quenched flavors are introduced as valence quarks using the Osterwalder-Seiler (OS) type action [18, 32]. Following the Refs. [18, 22, 23],

in the valence sector we introduce three twisted doublets,  $(u, d)$ ,  $(s, s')$  and  $(c, c')$  with masses  $\mu_l$ ,  $\mu_s$  and  $\mu_c$ , respectively. Within each doublet, the two valence quarks are regularized in the physical basis with Wilson parameters of opposite signs ( $r = -r' = 1$ ). The fermion action for the valence sector reads

$$S = (\bar{\chi}_u, \bar{\chi}_d) (D_W + m_{crit} + i\mu_l\gamma_5\tau_3) \begin{pmatrix} \chi_u \\ \chi_d \end{pmatrix} \\ + (\bar{\chi}_s, \bar{\chi}_{s'}) (D_W + m_{crit} + i\mu_s\gamma_5\tau_3) \begin{pmatrix} \chi_s \\ \chi_{s'} \end{pmatrix} \\ + (\bar{\chi}_c, \bar{\chi}_{c'}) (D_W + m_{crit} + i\mu_c\gamma_5\tau_3) \begin{pmatrix} \chi_c \\ \chi_{c'} \end{pmatrix}. \quad (8)$$

One can perform a chiral twist to transform the quark fields in physical basis to the so-called twisted basis as follows:

$$\begin{pmatrix} u \\ d \end{pmatrix} = \exp(i\omega\gamma_5\tau_3/2) \begin{pmatrix} \chi_u \\ \chi_d \end{pmatrix} \\ \begin{pmatrix} s \\ s' \end{pmatrix} = \exp(i\omega\gamma_5\tau_3/2) \begin{pmatrix} \chi_s \\ \chi_{s'} \end{pmatrix} \\ \begin{pmatrix} c \\ c' \end{pmatrix} = \exp(i\omega\gamma_5\tau_3/2) \begin{pmatrix} \chi_c \\ \chi_{c'} \end{pmatrix} \quad (9)$$

where  $\omega = \pi/2$  implements the full twist.

Two sets of gauge field ensembles are utilized in this work, each containing 200 gauge field configurations. We shall call them Ensemble I and II. The explicit parameters are listed in Table I. The corresponding renormalization factor  $Z_V(g_0^2)$  taken from Ref. [31] are also provided for these two ensembles. We have also taken the corresponding parameter  $\mu_c$  as indicated in that reference.

TABLE I. Parameters for the gauge ensembles used in this work. See Ref. [31] and references therein for notations.

Ensemble	$\beta$	$a[\text{fm}]$	$V/a^4$	$a\mu_{sea}$	$m_\pi[\text{MeV}]$	$a\mu_c$	$Z_V(g_0^2)$
I	3.9	0.085	$24^3 \times 48$	0.004	315	0.215	0.6103(3)
II	4.05	0.067	$32^3 \times 64$	0.003	300	0.185	0.6451(3)

For the meson operators, in the physical basis, we use simple quark bi-linears such as  $\bar{q}\Gamma q$  and the corresponding form in twisted basis will be denoted as  $\bar{\chi}_q\Gamma'\chi_q$  which can be readily obtained from Eq. (9). For later convenience, these are tabulated in table II together with the possible  $J^{PC}$  quantum numbers in the continuum and the names of the corresponding particle in the light and the charm sector. The current operators that appear in Eq. (7) are also listed.

## B. Twisted boundary conditions

In order to increase the resolution in momentum space, particularly close to the physical point of  $Q_1^2 = Q_2^2 = 0$ , it is customary to implement the twisted boundary

TABLE II. Local interpolating operators for vector and pseudo-scalar states and the current operators that appear in Eq. (7) in both physical and twisted basis,  $\bar{q}\Gamma q = \bar{\chi}_q\Gamma'\chi_q$ . The names of the corresponding particle and their  $J^{PC}$  quantum numbers in the continuum are also listed. The index for  $i$ ,  $\mu$  and  $\nu$  are 1, 2, 3.

	$\rho/J/\psi$	$\pi/\eta_c$	$j^\mu$	$j^\nu$
$\Gamma$	$\gamma_i$	$\gamma_5$	$\gamma_\mu$	$\gamma_\nu$
$\Gamma'$	$\gamma_i$	1	$\gamma_\mu$	$\gamma_\nu$
$J^{PC}$	$1^{--}$	$0^{-+}$	$1^{--}$	$1^{--}$

conditions (TBC) [31, 33–35] in recent lattice form factor computations, see e.g. [36]. We have also adopted the twisted boundary conditions for the valence quark fields, also known as partially twisted boundary conditions.

The quark field  $\psi_{\boldsymbol{\theta}}(\mathbf{x}, t)$ , when it is transported by an amount of  $L$  along the spatial direction  $i$  ( $i = 1, 2, 3$ ), will change by a phase factor  $e^{i\theta_i}$ ,

$$\psi_{\boldsymbol{\theta}}(\mathbf{x} + L\mathbf{e}_i, t) = e^{i\theta_i} \psi_{\boldsymbol{\theta}}(\mathbf{x}, t), \quad (10)$$

where  $\boldsymbol{\theta} = (\theta_1, \theta_2, \theta_3)$  is the twisted angle for the quark field in spatial directions which can be tuned freely. In this calculations, we only twist one of the charm quark field in both vector currents, the other charm quark fields remain un-twisted. If we introduce the new quark fields

$$\hat{c}'(\mathbf{x}, t) = e^{-i\boldsymbol{\theta} \cdot \mathbf{x}/L} c'_{\boldsymbol{\theta}}(\mathbf{x}, t), \quad (11)$$

It is easy to verify that  $\hat{c}'(\mathbf{x}, t)$  satisfy the conventional periodic boundary conditions along all spatial directions; i.e.,  $\hat{c}'(\mathbf{x} + L\mathbf{e}_i, t) = \hat{c}'(\mathbf{x}, t)$  with  $i = 1, 2, 3$  if the original field  $c'_{\boldsymbol{\theta}}(\mathbf{x}, t)$  satisfies the twisted boundary conditions (10). For Wilson-type fermions, this transformation is equivalent to the replacement of the gauge link; i.e.,

$$U_\mu(x) \Rightarrow \hat{U}_\mu(x) = e^{i\theta_\mu a/L} U_\mu(x), \quad (12)$$

for  $\mu = 0, 1, 2, 3$  and  $\theta_\mu = (0, \boldsymbol{\theta})$ . In other words, each spatial gauge link is modified by a  $U(1)$ -phase. Then the current vectors that appear in Eq. (7) are constructed using the hatted and the original charm quark field as,

$$\begin{cases} j^\nu(\mathbf{y}, t) = \bar{c}(\mathbf{y}, t)(\gamma_\nu)\hat{c}'(\mathbf{y}, t), \\ j^\mu(\mathbf{0}, t_i) = \bar{\hat{c}}'(\mathbf{0}, t_i)(\gamma_\mu)c(\mathbf{0}, t_i). \end{cases} \quad (13)$$

The allowed momenta on the lattice are thus modified to

$$\mathbf{q}_i = \left(\frac{2\pi}{L}\right) \left(\mathbf{n}_i + \frac{\boldsymbol{\theta}}{2\pi}\right), \quad (14)$$

for  $i = 1, 2$  where  $\mathbf{n}_i \in \mathbb{Z}^3$  is a three-dimensional integer. By choosing different values for  $\boldsymbol{\theta}$ , we could obtain more values of  $\mathbf{q}_1$  and  $\mathbf{q}_2$  than conventional periodic boundary conditions. In this paper, apart from the untwisted case of  $\boldsymbol{\theta} = (0, 0, 0)$ , we have also computed the following cases:  $\boldsymbol{\theta} = (0, 0, \pi)$ ,  $(0, 0, \pi/2)$ ,  $(0, 0, \pi/4)$  and  $(0, 0, \pi/8)$ . These choices offer us many more data points in the vicinity of the physical kinematic region.

### C. Meson spectrum and the dispersion relations

Before calculating the matrix element with two photon decay from  $\eta_c$ , the mass for  $\eta_c$  and  $\rho$  state and the energy dispersion relations for  $\eta_c$  must be verified. This is particularly important for our study due to the following reasons. Firstly, we use the  $N_f = 2$  twisted mass configurations, the sea quarks contains  $u$  and  $d$  quark field. For  $\rho$  state, it has the same quantum number with photon and it is the lightest vector meson in QCD. Then we should calculate the  $\rho$  mass to restrict the photon energy  $Q_1^2, Q_2^2 > -m_\rho^2$  on lattices which we used in this simulations. Secondly, although  $\eta_c$  spectrum has been studied extensively in lattice QCD and the overall picture agrees reasonably well with the experiment. Here, we want to compare the continuum dispersion relationship Eq. (16) with the lattice dispersion relationship Eq. (17) to choose one of them, and then calculate the input parameters.

Following Eq. (6), the energy  $E_{\eta_c}(\mathbf{p}_f)$  for  $\eta_c$  state with three-momentum  $\mathbf{p}_f$  can be obtained from the corresponding two-point function via

$$\cosh(E_{\eta_c}(\mathbf{p}_f)) = \frac{C(\mathbf{p}_f; t-1) + C(\mathbf{p}_f; t+1)}{2C(\mathbf{p}_f; t)} \quad (15)$$

The two point function is symmetric about  $t = T/2$ . In real simulation we average the data from two halves about  $t = T/2$  to improve statistics. We use the effective mass plateaus at zero three-momentum for the  $\eta_c$  and  $\rho$  state to obtain the masses which are then listed in Table III. The mass of the  $\eta_c$  comes out to be lighter than its physical value since these values are still finite lattice spacing values. When extrapolated towards the continuum limit, the mass will become compatible with the experimental value. The mass of the  $\rho$  here serves to restrict our kinematic regions where analytic continuation is justified.

TABLE III. The meson mass values for  $\eta_c$  and  $\rho$  obtained from the two ensembles in this work.

Ensemble	$m_{\eta_c} [\text{MeV}]$	$m_\rho [\text{MeV}]$
I	2678(3)	903(88)
II	2812(2)	1051(50)

Similarly, we obtain the energies for  $\eta_c$  at non-vanishing momenta via Eq. (15) which then can be utilized to verify the the following two dispersion relations: the conventional one in the continuum,

$$E^2(\mathbf{p}) = m^2 + Z_{\text{cont}} \cdot \sum_i p_i^2, \quad (16)$$

and its lattice counterpart,

$$4 \sinh^2 \frac{E(\mathbf{p})}{2} = 4 \sinh^2 \frac{m}{2} + Z_{\text{latt}} \cdot 4 \sum_i \sin^2 \left( \frac{p_i}{2} \right). \quad (17)$$

For free particles, the constants  $Z_{\text{cont}}$  and  $Z_{\text{latt}}$  should be close to unity. In Fig. 1, we show this comparison

for the two dispersion relations for the  $\eta_c$  state. In the left/right panel, the dispersion relations are illustrated using continuum/lattice dispersion relations, respectively. For the continuum dispersion relation, the horizontal axis is simply  $\mathbf{p}^2$  while for the lattice dispersion relation,  $\hat{\mathbf{p}}^2 = 4 \sum_i \sin^2(p_i/2)$  is plotted. In both panels, points with errors are from simulations on  $32^3 \times 64$  (open circles) or  $24^3 \times 48$  (stars) lattices, respectively. Straight lines are the corresponding linear fits to these data. It is seen that, although both dispersion relations can be fitted nicely using linear fits, the slope for the continuum dispersion relation, i.e.  $Z_{\text{cont}}$  is very different from unity while its lattice counterpart  $Z_{\text{latt}}$  is close. This suggests that, for the  $\eta_c$  state, we should use the lattice dispersion relations instead of the naive continuum dispersion relation. This is not surprising since  $\eta_c$  is quite heavy in lattice units (close to unity). This modification of the dispersion relation does have consequences on our determination of the hadronic matrix element. We will come to this point again when we discuss form factor parametrization in the next subsection, see discussion after Eq. (18).

The following notations will be utilized. First of all, in the continuum, we will use  $q_{1,2}$  to designate the four-momentum of the photons. We will also use  $\omega_{1,2}$  to denote the temporal component of  $q_{1,2}$ , i.e.  $\omega_{1,2} \equiv q_{1,2}^0$ . When the photons are on-shell, we have  $\omega_{1,2} = |\mathbf{q}_{1,2}|$  with  $\mathbf{q}_{1,2}$  being the corresponding three-momentum. The so-called virtuality of the photons are defined as the corresponding four-momentum squared:  $Q_{1,2}^2 \equiv (-q_{1,2}^2)$ . On the lattice, there are also lattice counterparts of the above notations, arising from the lattice dispersion relation (17). For that we simply add a hat on the corresponding variable. For example, we will use  $\hat{\omega}_1 = 2 \sinh(\omega_1/2)$  to denote the lattice version of  $\omega_1$ .

The computation has to cover the physical interesting kinematic region. For this purpose, we have to scan the corresponding parameter space. We basically follow the following strategy: We first fix the four-momentum of  $\eta_c$ ,  $p_f = (E_{\eta_c}, \mathbf{p}_f)$ , and place it on a given time-slice  $t_f = T$ . Note that we just have to fix  $\mathbf{p}_f = \mathbf{n}_f(2\pi/L)$  and  $E_{\eta_c}$  can be obtained from the dispersion relation (17). This effectively puts  $\eta_c$  on-shell. Here we also have the freedom to pick a value for the twist angle  $\theta$ . Then, we judiciously choose several values of virtuality  $Q_1^2$  around the physical point  $Q_1^2 = 0$ . To be specific, we picked the range  $Q_1^2 \in [-0.5, +0.5] \text{ GeV}^2$ , which satisfies the constraint  $Q_1^2 > -m_\rho^2$ .<sup>1</sup> Since  $\mathbf{p}_f = \mathbf{q}_1 + \mathbf{q}_2$ , this means that, for a given  $\mathbf{p}_f$ , a choice of  $\mathbf{q}_1$  completely specifies  $\mathbf{q}_2$  and vice versa. We therefore take several choices of  $\mathbf{q}_1 = \mathbf{n}_1(2\pi/L)$  by changing three-dimensional integer  $\mathbf{n}_1$ . At this stage, we can compute the energy of the first photon  $\omega_1$ , since  $\omega_1^2 = \mathbf{q}_1^2 - Q_1^2$ . It turns out that we can also compute the virtuality of the second photon,

<sup>1</sup> This is valid with the physical  $\rho$  meson mass. Our lattice values yield a less stringent constraint.

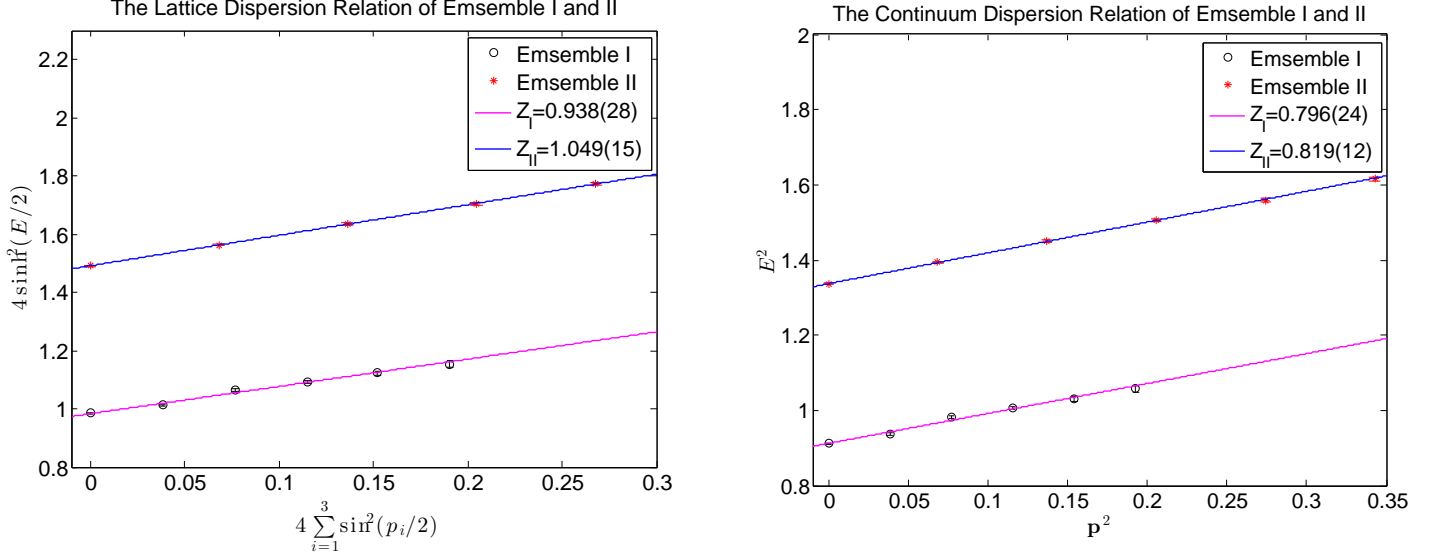


FIG. 1.  $\eta_c$  meson dispersion relation obtained from simulations on Ensemble I (crosses) and Ensemble II (open circles). In the left/right panel, the horizontal axis represents the continuum/lattice three-momentum squared variable. Straight lines in both panels are the corresponding linear fits using continuum/lattice dispersion relations Eq. (16) or Eq. (17). The fitted parameters  $Z_{\text{cont}}$  and  $Z_{\text{latt}}$  together with their errors are also shown.

$Q_2^2 = |\mathbf{q}_2|^2 - \omega_2^2$ , since  $\omega_2 = E_{\eta_c} - \omega_1$  and  $\mathbf{q}_2$  is also known by the choice of  $\mathbf{q}_1$ . One has to make sure that, the values of  $Q_2^2$  thus computed do satisfy the constraint  $Q_2^2 > -m_\rho^2$  otherwise it is omitted. This procedure is summarized as follows:

1. Pick  $\mathbf{p}_f$  and  $\boldsymbol{\theta}$ . Obtain  $E_{\eta_c}(\mathbf{p}_f)$  from dispersion relation (17);
2. Judiciously choose several values of  $Q_1^2$  in a suitable range, say  $Q_1^2 \in [-0.5, +0.5]\text{GeV}^2$ ;
3. Pick values of  $\mathbf{n}_1$  such that  $\mathbf{q}_1 = \mathbf{n}_1(2\pi/L)$ . This fixes both  $\omega_1$  and  $Q_2^2$ , using energy-momentum conservation;
4. Make sure all values of  $Q_1^2, Q_2^2 > -m_\rho^2$ , otherwise the choice is simply ignored;
5. For each validated choice above, compute the three-point functions (7), the two-point functions (6) and eventually obtain the hadronic matrix element using Eq. (5).

#### D. Form factors for $\eta_c$

In order to compute the desired hadronic matrix element  $\langle \eta_c(p_f) | \gamma(q_1, \lambda_1) \gamma(q_2, \lambda_2) \rangle$  in Eq. (5), we choose to place  $\eta_c$  state at a fixed sink position  $t_f = T$ . This sink position is then used as a sequential source for a backward charm propagator inversion. We compute this with all possible source positions  $t_i$  and insertion point  $t$ . This method allows us to freely vary the value of  $\omega_1$ ,  $Q_1^2$  (as

discussed in previous subsection) and to directly inspect the behavior of the integrand in Eq. (5).

Taking  $\mathbf{p}_f = \mathbf{0}$  for the  $\eta_c$  state as an example,, we show the behavior of the integrand in Fig. 2 for insertion positions  $t = 4, 8, 12, 16, 20$  for ensemble I and  $t = 4, 8, 12, 16, 20, 24, 28$  for ensemble II. It is seen that the integrand is peaked around  $t_i = t$ , making the contributions close to this point the dominant part of the matrix element. For the lattice theory, the integration of  $t_i$  in Eq. (5) is replaced by a summation.

The matrix element  $\langle \eta_c | \gamma(q_1, \lambda_1) \gamma(q_2, \lambda_2) \rangle$  can be parameterized using the form factor  $F(Q_1^2, Q_2^2)$  as follows,

$$\langle \eta_c | \gamma(q_1, \lambda_1) \gamma(q_2, \lambda_2) \rangle = 2(\frac{2}{3}e)^2 m_{\eta_c}^{-1} F(Q_1^2, Q_2^2) \epsilon_{\mu\nu\rho\sigma} \times \epsilon^\mu(q_1, \lambda_1) \epsilon^\nu(q_2, \lambda_2) q_1^\rho q_2^\sigma, \quad (18)$$

where  $\epsilon^\mu(q_1, \lambda_1), \epsilon^\nu(q_2, \lambda_2)$  are the polarization vectors of the photons while  $q_1$  and  $q_2$  are the corresponding four-momenta. Here one should be careful about the form of the momenta to use. Recall that these momentum factors originate from derivatives in the continuum. On the lattice, they should be replaced by the corresponding finite differences, i.e. one should use the lattice version of the momentum:  $q^0 \rightarrow 2 \sinh(q^0/2)$  and  $q^i \rightarrow 2 \sin(q^i/2)$ . Since the spatial momenta that we are using are relatively small in lattice units, the effect of this replacement might be optional. However, for the 0-th component, since each of the photon is roughly half of the  $\eta_c$  energy which is large in lattice units as we discussed in subsection III C, this replacement does make a difference.

According to Eq. (5), the matrix element and therefore also the form factor  $F(Q_1^2, Q_2^2)$  should be independent of the insertion point  $t$ . We indeed observe this plateau behavior in our data which is illustrated in Fig. 3 for the

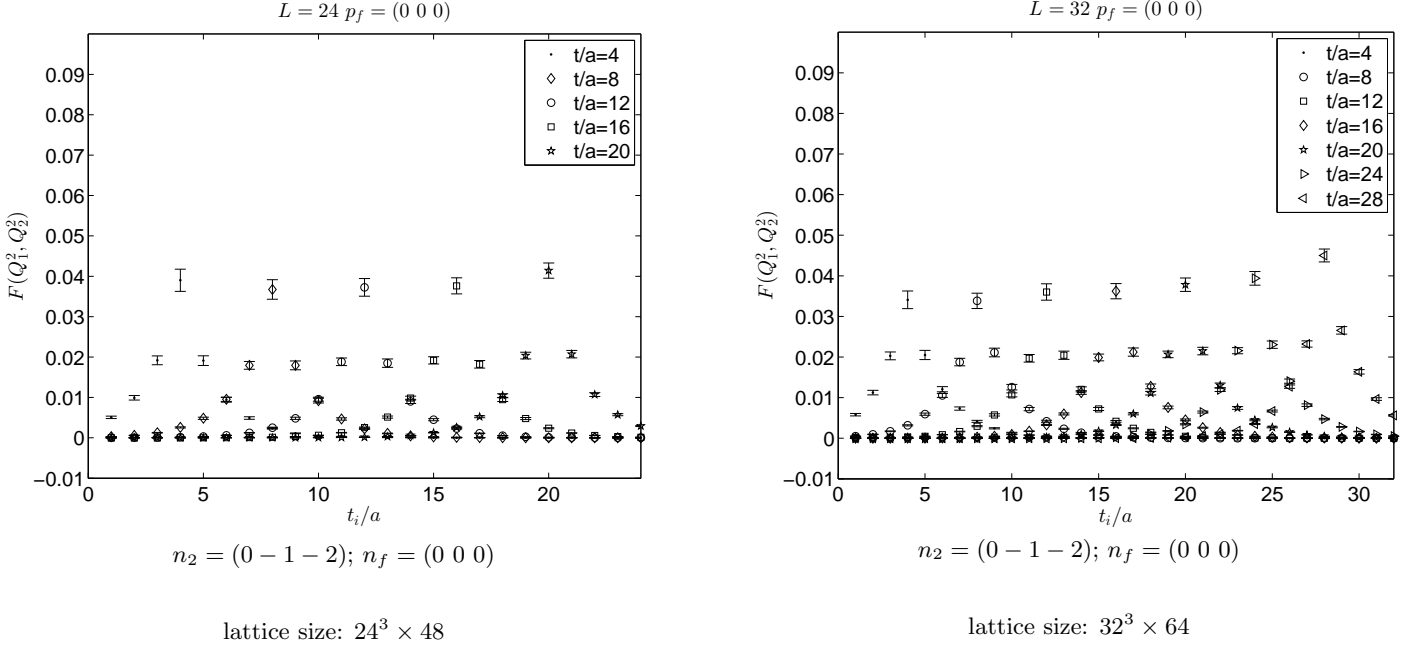


FIG. 2. The integrand in Eq. (5) versus  $t_i$  for various insertion points  $t$  obtained from our simulation with ensemble I (left panel), and ensemble II (right panel). We take  $\mathbf{n}_2 = (0, -1, -2)$ ;  $\mathbf{n}_f = (0, 0, 0)$  in this example. The insertion points are  $t = 4, 8, 12, 16, 20$  and  $t = 4, 8, 12, 16, 20, 24, 28$  for ensemble I and II, respectively.

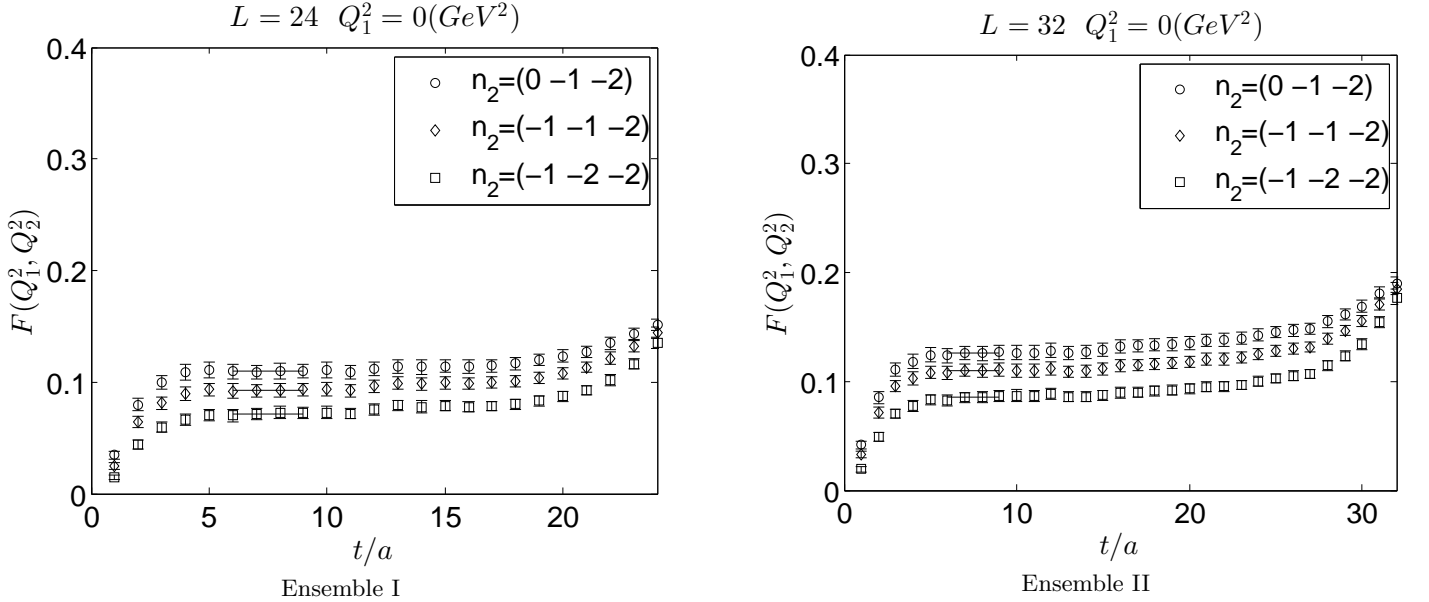


FIG. 3. The plateau of the form factor obtained by an integration (summation) over  $t_i$  for three-point function  $G_{\mu\nu}(t_i, t)$  with ensemble I (left panel) and ensemble II (right panel). We take  $Q_1^2 = 0$ ;  $n_f = (0, 0, 0)$  in this particular plot. Different data points correspond to different choices of  $\mathbf{n}_2$  as indicated.

case of  $Q_1^2 = 0$  as an example. Other cases are similar. Fitting these plateaus then yields the corresponding values for the matrix element  $\langle \eta_c | \gamma(q_1, \lambda_1) \gamma(q_2, \lambda_2) \rangle$  or equivalently the form factor  $F(Q_1^2, Q_2^2)$ .

To describe the virtuality dependence of the form factor, we adopt a simple one-pole parametrization to fit

our data.

$$F(Q_1^2, Q_2^2) = F(Q_1^2, 0) / (1 + Q_2^2 / \mu^2(Q_1^2)), \quad (19)$$

where  $F(Q_1^2, 0)$  and  $\mu^2(Q_1^2)$  are regarded as the fitting parameters at the given value of  $Q_1^2$ . Since measurements at different values of  $Q_1^2$  or  $Q_2^2$  are all obtained on the same set of ensembles, we adopt the correlated fits, taking into

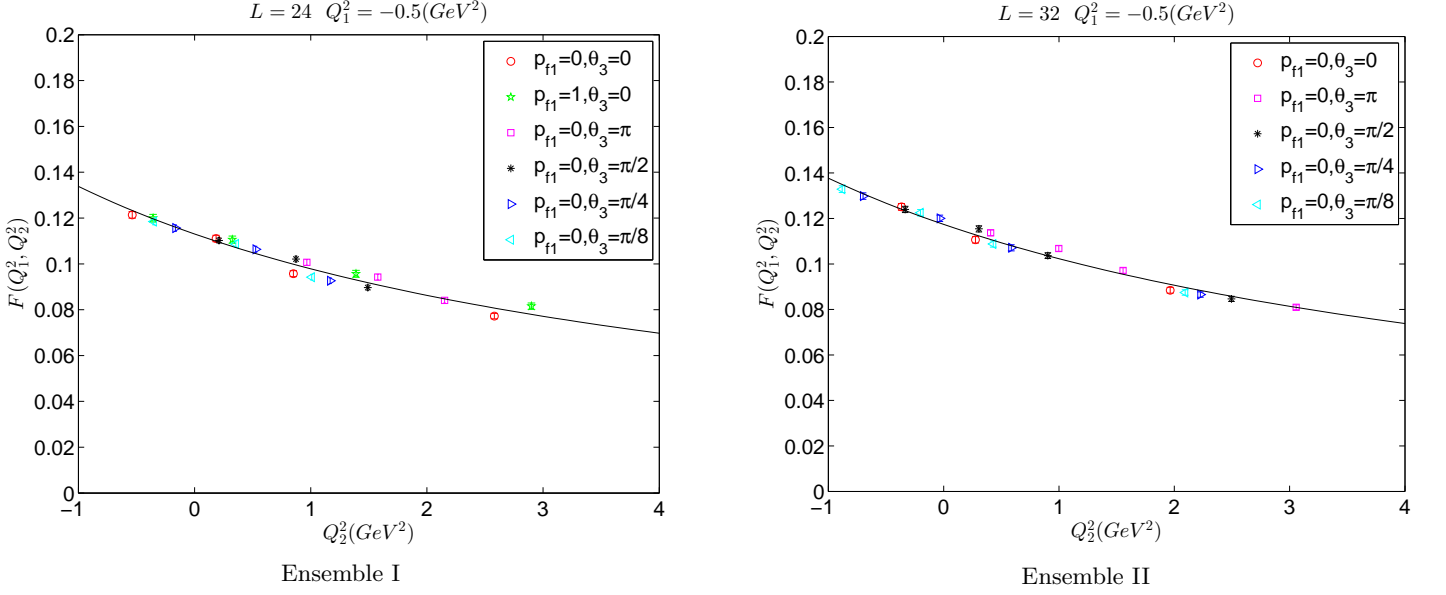


FIG. 4. The fitted results for  $F(Q_1^2, Q_2^2) = F(Q_1^2, 0)/(1 + Q_2^2/\mu^2(Q_1^2))$  by one-pole form factor for Ensemble I (left figure) and Ensemble II (right figure) at a fixed value of  $Q_1^2 = -0.5\text{GeV}^2$ . Different data points correspond to different parameter combinations as indicated in the Figure.  $p_{f1}$  denotes x-component of the momentum  $\mathbf{p}_f$  of  $\eta_c$ , and  $\theta_3$  represents z-component of twisted angle  $\theta$ .

account possible correlations among different  $Q^2$  values. The covariance matrix among them are estimated using a bootstrap method.

As an example, taking  $Q_1^2 = -0.5\text{GeV}^2$ , the fitting results are shown in Fig. 4. It is seen that this simple formula describes the data rather well even for quite large values of  $Q_2^2$ . We therefore have taken all available values of  $Q_2^2$  into the fitting process. Notice also that, by using the twisted boundary conditions together with different combinations of the lattice momenta, we are able to populate the physical region close to  $Q_1^2 = Q_2^2 = 0$  rather effectively. We have tried both correlated and uncorrelated fits on our data. The central values for the fitted parameters are compatible, however, the error estimates are somewhat different. We adopt the correlated fits as our final results. Fits for other set of parameters are similar and the final results are summarized in Table IV for reference.

Having obtained the results for  $F(Q_1^2, 0)$ , we can fit it again with another one-pole form,

$$F(Q_1^2, 0) = F(0, 0)/(1 + Q_1^2/\nu^2). \quad (20)$$

with  $F(0, 0)$  and  $\nu^2$  being the fitting parameters. This is illustrated in Fig. 5 for two of our ensembles. Again, correlated fits are adopted here.

The on-shell decay width  $\Gamma$  for  $\eta_c$  to two physical photons is related to the form factor  $F(0, 0)$  via

$$\Gamma = \pi\alpha_{em}^2 \frac{16}{81} m_{\eta_c} |F(0, 0)|^2, \quad (21)$$

where  $\alpha_{em} \simeq 1/137$  is the fine structure constant. When computing this decay width, however, one has to plug in the mass of the  $\eta_c$  meson. What we really

compute on the lattice is the combination of correlation functions which is related to the matrix element  $\langle \eta_c | \gamma(q_1, \lambda_1) \gamma(q_2, \lambda_2) \rangle$  via Eq. (5). When we parameterize this particular matrix element in terms of form factor in Eq. (18), the relation involves  $m_{\eta_c}$  as well. Therefore, the decay width turns out to be proportional to  $m_{\eta_c}^3$ :  $\Gamma \propto m_{\eta_c}^3 |\langle \eta_c | \gamma(q_1, \lambda_1) \gamma(q_2, \lambda_2) \rangle|^2$ . Here it is then quite different if one substitutes in the value of  $m_{\eta_c}$  obtained on the lattice, or the true physical value of  $m_{\eta_c}^{\text{phys.}} = 2.98\text{GeV}$ , the two differs by about 10% for the coarser lattice and about 5% for the finer lattice. Therefore, if one would substitute in the true physical mass, it will result in a 15% difference in the value of  $\Gamma$  for the finer lattice.

The reason for the above mentioned difference is the following. We are taking the value of the valence charm quark mass parameter  $\mu_c$  from Ref. [31]. There, it is assumed that, when the continuum limit is taken, the value of  $m_{\eta_c}$  will recover its physical value. However, being on a finite lattice, the computed value of  $m_{\eta_c}$  comes out to be less than the corresponding physical value. The difference of the two is in fact an estimate of the finite lattice spacing error. In fact,  $m_{\eta_c}$  is not the only factor which affects the results. The renormalization factor  $Z_V(g_0^2)$  that we quoted in Table I also depends on the lattice spacing. Therefore, we think it is more consistent to substitute in the values of  $m_{\eta_c}$  computed on each ensembles. In the end, of course, one should try to take the continuum limit when the lattice computations are performed on a set of ensembles with different lattice spacings. Using Eq. (21) with the values of  $m_{\eta_c}$  obtained from each ensemble substituted in, we obtain for the decay width



TABLE IV. The summary of fitted results for  $F(Q_1^2, 0)$  and  $\mu^2(Q_1^2)$  using Eq. (19) for Ensemble I (left four columns) and Ensemble II (right four column). The corresponding  $\chi^2/dof$  are also presented.

Ensemble I				Ensemble II			
$Q_1^2(GeV^2)$	$F(Q_1^2, 0)$	$\mu^2(Q_1^2)(GeV^2)$	$\chi^2/dof$	$Q_1^2(GeV^2)$	$F(Q_1^2, 0)$	$\mu^2(Q_1^2)(GeV^2)$	$\chi^2/dof$
-0.5	0.113(12)	6.4(4.9)	0.092/18	-0.5	0.1173(97)	6.7(3.7)	0.065/18
-0.4	0.111(11)	6.5(4.8)	0.092/18	-0.4	0.115(10)	6.7(3.8)	0.058/17
-0.3	0.109(10)	6.6(4.7)	0.091/18	-0.3	0.114(10)	6.6(4.1)	0.053/16
-0.2	0.107(10)	6.5(4.9)	0.090/17	-0.2	0.1128(98)	6.7(4.0)	0.052/16
-0.1	0.105(10)	6.6(4.8)	0.089/17	-0.1	0.111(10)	6.7(4.3)	0.047/15
0	0.104(11)	6.6(5.5)	0.087/15	0	0.1098(97)	6.8(4.2)	0.047/15
0.1	0.102(11)	6.5(6.0)	0.084/14	0.1	0.1081(93)	6.9(4.1)	0.047/15
0.2	0.101(10)	6.6(5.8)	0.082/14	0.2	0.106(10)	6.9(4.7)	0.044/13
0.3	0.099(10)	6.7(5.7)	0.083/14	0.3	0.105(10)	7.0(5.1)	0.043/12
0.4	0.0979(94)	6.8(5.5)	0.083/14	0.4	0.103(10)	7.1(5.0)	0.043/12
0.5	0.0963(10)	6.8(6.5)	0.083/12	0.5	0.102(10)	7.2(5.4)	0.043/11

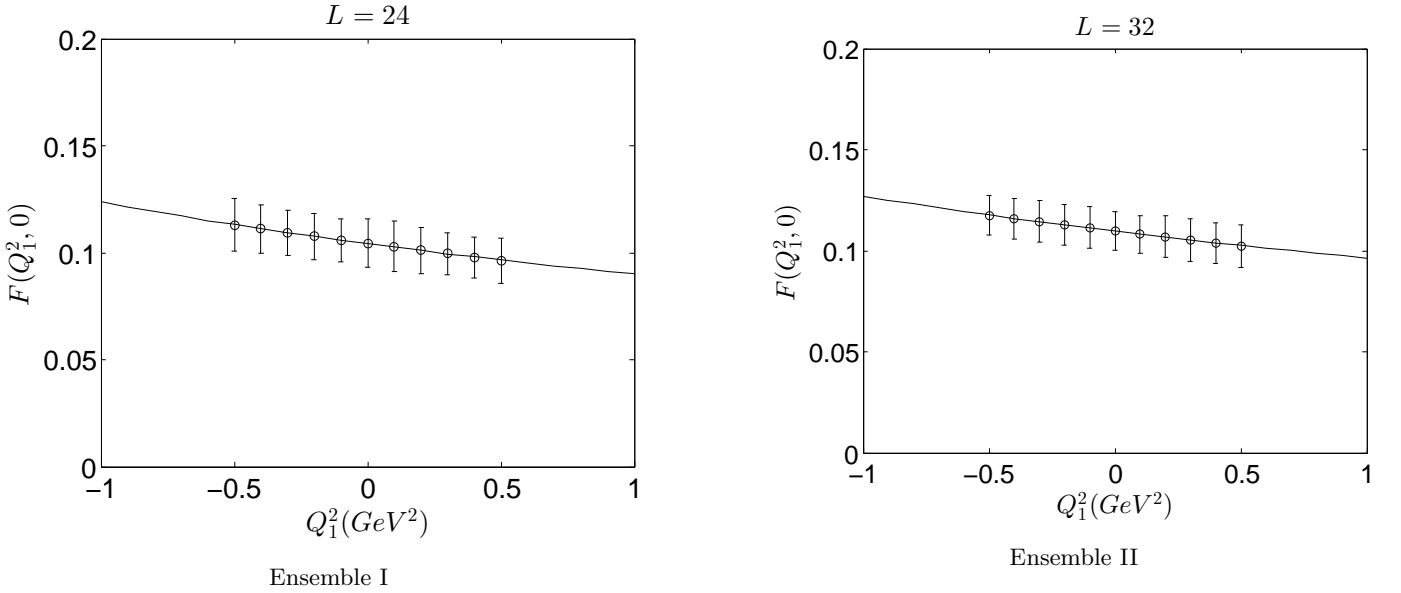


FIG. 5.  $F(Q_1^2, 0)$  is again fitted with a one-pole form:  $F(Q_1^2, 0) = F(0, 0)/(1 + Q_1^2/\nu^2)$  for Ensemble I (left figure) and Ensemble II (right figure).

$\Gamma = 0.961(59)\text{KeV}$  for the coarser and  $\Gamma = 1.113(63)\text{KeV}$  for the finer lattice ensembles. Finally, the fitted results for  $F(0, 0)$  together with the corresponding results for the decay width are summarized in Table V.

Let us now discuss the possible systematic errors. Although the mass of the pion in the two ensembles are relatively heavy, we do not expect the double photon decay width to be very sensitive to the pion mass. Also, since both of our ensembles have  $m_\pi L \sim 3.3$ , we do not expect very large finite volume errors as well. Since we have only two ensembles, it is not possible to make reliable extrapolation towards the continuum limit. However, if one would try a naive continuum limit extrapolation, assuming an  $\mathcal{O}(a^2)$  error, we obtain  $\Gamma = 1.36(19)\text{KeV}$  which is also listed in Table V. There are of course other sources of systematic errors, e.g. the neglecting of the so-called

disconnected contributions, the quenching of the strange quark, etc. Therefore, we decided not to quantify the systematic errors in this exploratory study.

Now let us briefly discuss the implications of our lattice results for  $\Gamma$ . First of all, our results are smaller than, but marginally compatible with the quenched lattice result in Ref. [17]. They obtained  $\Gamma = 2.65(26)\text{stat}(80)\text{scal.}(53)\text{quen. KeV}$ , where we have added their error estimates in quadrature. The possible reasons are that we have used different configurations in the simulations, and the chosen configurations simulated in this paper are dynamical for  $N_f = 2(u, d \text{ quarks})$ . This is to say, these configurations contain sea quarks and loops of sea quark contributions. While, in Ref. [17], quenched configurations were used, where the contributions from loops of the sea quark have been ignored.

TABLE V.  $F(Q_1^2, 0)$  is again fitted with a one-pole form:  $F(Q_1^2, 0) = F(0, 0)/(1 + Q_1^2/\nu^2)$  are shown for the two ensembles (the first two lines). In the last column, we show the decay width obtained using Eq. (21). A naive continuum extrapolation are shown in the third line for reference.

	$F(0, 0)$	$\nu^2 (GeV^2)$	$\chi^2/dof$	$\Gamma(\eta_c \rightarrow \gamma\gamma) (KeV)$
Ensemble I	0.1041(32)	6.3(3.9)	0.0021/9	0.961(59)
Ensemble II	0.1096(31)	7.2(4.6)	0.0035/9	1.113(63)
Naive extrapolation				1.36(19)

Second, our final results for  $\Gamma$  from both of our lattice ensembles turn out to be smaller than the current PDG value, which is about 5.0 KeV with an error of 0.4 KeV. We have also not quantified the systematic errors which is not possible for an exploratory study. However, as we discussed already, the difference in the  $\eta_c$  mass indicates that there might be a finite lattice spacing error at the order of 15%. Also missing in this study is the so-called disconnected contributions which are costly even to estimate. Needless to say, a more systematic study using more ensembles of configurations will be helpful to clarify these issues.

#### IV. CONCLUSIONS

In this exploratory study, we calculate the decay width for two-photon decay of  $\eta_c$  using unquenched  $N_f = 2$  twisted mass fermions. The computation is done with two lattice ensembles (coarser and finer) at two different lattice spacings. The mass spectrum and dispersion relations for the  $\eta_c$  state are first examined. It is verified that lattice dispersion relations are better than the continuum ones. The implication of this is carried over to the computation of hadronic matrix element and the corresponding form factor.

By calculating various three-point functions, two-photon decays of  $\eta_c$  matrix element are obtained at various of virtualities. It is particularly helpful to implement the so-called twisted boundary conditions. The matrix element is decomposed into kinematic factors and one form factor  $F(Q_1^2, Q_2^2)$  which is obtained in a region close to the physical one. Then, we adopt a simple one-pole parametrization to fit the data for each value of  $Q_1^2$ , and subsequently fit  $F(Q_1^2, 0)$  again with a one-pole form yielding the value of  $F(0, 0)$ . We finally obtain  $\Gamma = 0.961(59)KeV$  for the coarser and  $\Gamma = 1.113(63)KeV$  for the finer lattice ensembles. A naive continuum extrap-

olation gives  $\Gamma = 1.36(19)KeV$  which is compared with the previous quenched lattice result and the PDG result. Our result is significantly smaller than both. However, taking into account of the possibly large systematic errors in the present lattice computations and the large uncertainties in the experimental result itself, it is still premature to say that there is a discrepancy here. Obviously, future more systematic lattice studies with various lattice spacings and more statistics are very much welcome here. It would also be helpful to estimate the disconnected contributions that has been neglected in this exploratory study. Last but not the least, more precise experimental results on double photon decays of charmonium are crucial in this area as well.

#### ACKNOWLEDGMENTS

The authors would like to thank the European Twisted Mass Collaboration (ETMC) to allow us to use their gauge field configurations. Our thanks also go to National Supercomputing Center in Tianjin (NSCC) and the Bejing Computing Center (BCC) where part of the numerical computations are performed. This work is supported in part by the National Science Foundation of China (NSFC) under the project No.11505132, No.11335001, No.11275169, No.11405178, No.11105153. It is also supported in part by the DFG and the NSFC (No.11261130311) through funds provided to the Sino-Germen CRC 110 ‘‘Symmetries and the Emergence of Structure in QCD’’. This work is also funded in part by National Basic Research Program of China (973 Program) under code number 2015CB856700. M. Gong and Z. Liu are partially supported by the Youth Innovation Promotion Association of CAS (2013013, 2011013). This work is also supported by the Scientific Research Program Funded by Shanxi Provincial Education Department under the grant No. 15JK1348.

- 
- |  |  |
|--|--|
| <p>[1] D. Diakonov, M. G. Ryskin, and A. G. Shuvaev, JHEP <b>02</b>, 069 (2013), arXiv:1211.1578 [hep-ph].</p> <p>[2] J. P. Lees et al. (BaBar), Phys. Rev. <b>D81</b>, 052010 (2010), arXiv:1002.3000 [hep-ex].</p> <p>[3] T. N. Pham, Nucl. Phys. Proc. Suppl. <b>234</b>, 291 (2013).</p> <p>[4] V. Savinov (Belle), Nucl. Phys. Proc. Suppl. <b>234</b>, 287 (2013).</p> | <p>[5] M. Ablikim et al. (BESIII), Phys. Rev. <b>D85</b>, 112008 (2012), arXiv:1205.4284 [hep-ex].</p> <p>[6] P. Guo, T. Ypez-Martinez, and A. P. Szczepaniak, Phys. Rev. <b>D89</b>, 116005 (2014), arXiv:1402.5863 [hep-ph].</p> <p>[7] O. Bondareko (BESIII), PoS <b>QNP2012</b>, 091 (2012).</p> <p>[8] G. Li and Q. Zhao, Phys. Rev. <b>D84</b>, 074005 (2011), arXiv:1107.2037 [hep-ph].</p> |
|--|--|

- [9] Y. Chen *et al.*, Phys. Rev. **D84**, 034503 (2011), arXiv:1104.2655 [hep-lat].
- [10] U.-G. Meissner, Int. J. Mod. Phys. Conf. Ser. **02**, 56 (2011).
- [11] C. E. Thomas (Hadron Spectrum), Chin. Phys. **C34**, 1512 (2010).
- [12] C. E. Thomas (Hadron Spectrum), AIP Conf. Proc. **1257**, 77 (2010).
- [13] Y.-P. Kuang, T. Barnes, C. Yuan, and H.-X. Chen, Int. J. Mod. Phys. **A24S1**, 327 (2009).
- [14] J. J. Dudek, R. Edwards, and C. E. Thomas, Phys. Rev. **D79**, 094504 (2009), arXiv:0902.2241 [hep-ph].
- [15] X.-d. Ji and C.-w. Jung, Phys. Rev. Lett. **86**, 208 (2001), arXiv:hep-lat/0101014 [hep-lat].
- [16] X.-d. Ji and C.-w. Jung, Phys. Rev. **D64**, 034506 (2001), arXiv:hep-lat/0103007 [hep-lat].
- [17] J. J. Dudek and R. G. Edwards, Phys. Rev. Lett. **97**, 172001 (2006), arXiv:hep-ph/0607140 [hep-ph].
- [18] R. Frezzotti and G. C. Rossi, JHEP **10**, 070 (2004), arXiv:hep-lat/0407002 [hep-lat].
- [19] A. Shindler, Phys. Rept. **461**, 37 (2008), arXiv:0707.4093 [hep-lat].
- [20] P. Boucaud *et al.* (ETM), Phys. Lett. **B650**, 304 (2007), arXiv:hep-lat/0701012 [hep-lat].
- [21] P. Boucaud *et al.* (ETM), Comput. Phys. Commun. **179**, 695 (2008), arXiv:0803.0224 [hep-lat].
- [22] B. Blossier *et al.* (European Twisted Mass), JHEP **04**, 020 (2008), arXiv:0709.4574 [hep-lat].
- [23] B. Blossier *et al.* (ETM), JHEP **07**, 043 (2009).
- [24] R. Baron *et al.*, JHEP **06**, 111 (2010), arXiv:1004.5284 [hep-lat].
- [25] R. Baron *et al.* (ETM), JHEP **08**, 097 (2010), arXiv:0911.5061 [hep-lat].
- [26] C. Alexandrou *et al.* (European Twisted Mass), Phys. Rev. **D78**, 014509 (2008), arXiv:0803.3190 [hep-lat].
- [27] C. Alexandrou, R. Baron, J. Carbonell, V. Drach, P. Guichon, K. Jansen, T. Korzec, and O. Pene (ETM), Phys. Rev. **D80**, 114503 (2009), arXiv:0910.2419 [hep-lat].
- [28] K. Jansen, A. Shindler, C. Urbach, and I. Wetzorke (XLF), Phys. Lett. **B586**, 432 (2004), arXiv:hep-lat/0312013 [hep-lat].
- [29] B. Blossier, P. Dimopoulos, R. Frezzotti, V. Lubicz, M. Petschlies, F. Sanfilippo, S. Simula, and C. Tarantino (ETM), Phys. Rev. **D82**, 114513 (2010), arXiv:1010.3659 [hep-lat].
- [30] R. Frezzotti, S. Sint, and P. Weisz (ALPHA), JHEP **07**, 048 (2001), arXiv:hep-lat/0104014 [hep-lat].
- [31] D. Becirevic and F. Sanfilippo, JHEP **01**, 028 (2013), arXiv:1206.1445 [hep-lat].
- [32] K. Osterwalder and E. Seiler, Annals Phys. **110**, 440 (1978).
- [33] P. F. Bedaque, Phys. Lett. **B593**, 82 (2004), arXiv:nucl-th/0402051 [nucl-th].
- [34] C. T. Sachrajda and G. Villadoro, Phys. Lett. **B609**, 73 (2005), arXiv:hep-lat/0411033 [hep-lat].
- [35] S. Ozaki and S. Sasaki, Phys. Rev. **D87**, 014506 (2013), arXiv:1211.5512 [hep-lat].
- [36] B. B. Brandt, S. Capitani, M. Della Morte, D. Djukanovic, J. Gegelia, G. von Hippel, A. Juttner, B. Knippschild, H. B. Meyer, and H. Wittig, Eur. Phys. J. ST **198**, 79 (2011), arXiv:1106.1554 [hep-lat].